CSI-BASED CROSS-DOMAIN ACTIVITY RECOGNITION VIA ZERO-SHOT PROTOTYPICAL NETWORKS

A PREPRINT

Guillermo Diaz*
Dept. Communications Engineering
University of the Basque Country (UPV/EHU)
Bilbao, Spain
guillermo.diaz@ehu.eus

Iker Sobron
Dept. of Computer Languages and Systems
University of the Basque Country (UPV/EHU)
Bilbao, Spain
iker.sobron@ehu.eus

Iñaki Eizmendi
Dept. Communications Engineering
University of the Basque Country (UPV/EHU)
Bilbao, Spain
inaki.eizmendi@ehu.eus

Iratxe Landa
Dept. Communications Engineering
University of the Basque Country (UPV/EHU)
Bilbao, Spain
iratxe.landa@ehu.eus

Manuel Velez
Dept. Communications Engineering
University of the Basque Country (UPV/EHU)
Bilbao, Spain
manuel.velez@ehu.eus

December 13, 2023

ABSTRACT

The cross-domain capability of wireless sensing is currently one of the major challenges on human activity recognition (HAR) based on the channel state information (CSI) of wireless signals. The difficulty of labeling samples from new domains has encouraged the use of few and zero shot strategies. In this context, prototype networks have attracted attention due to their reasonable cross-domain transferability. This paper presents a novel zero-shot prototype recurrent convolutional network that implements a zero-shot learning strategy for HAR via CSI. This method extracts the prototypes from an available source domain to classify unseen and unlabeled data from the target domain for the same or similar classes. The experiments have been developed using three datasets with real measurements, and the results include an inter-datasets evaluation. Overall, the results improve the state of the art and make it a promising solution for cross-domain HAR.

1 Introduction

Wireless Sensing is a widely developed discipline due to its ability to digitize and sensorize environments. The vast extension of WiFi networks across the planet is seen as one of the primary keys to this technology, which has already implemented its hardware all over the globe. As WiFi networks are often used indoors, one of the essential elements in the future is the sensorization of indoor environments, where the Internet of Things tools play a crucial role in order to get smart environments. One of the most interesting proposals in this regard is to use home routers not only to transmit/receive data but also to analyze variations in the propagation channel to obtain information about the environment. In this sense, IEEE 802.11 has approved a new technical group called IEEE 802.11bf to accommodate sensing operations [1]. One area of interest in wireless sensing is Human Activity Recognition (HAR). Detecting

*Corresponding author

how many people are in an indoor location and what activities they are engaged in using WiFi signals can have many applications in different sectors such as home care, tourism, retail or security. Due to this, HAR is an important field of wireless sensing, ranging in several areas such as crowd counting[2, 3], people localization [4, 5, 6, 7], vital sign detection[8, 9, 10], and gesture recognition [11, 12, 13, 14, 15, 16, 17, 18, 19].

Technically, the HAR information comes from the variations of the propagation channel of the WiFi signals. These channel variations are calculated by the receiver, which measures the channel frequency response of the channel and generates the channel state information (CSI). Concretely, OFDM systems, such as WiFi, provide the CSI for antenna pairs between receiver and transmitter devices. CSI provides subcarrier-level channel measurements, generally used as a input data in HAR. However, raw CSI data usually need calibrations to achieve an exemplary system capable of providing HAR information.

The CSI consists of complex values representing an estimation of the wireless channel variations through which the waves are transmitted, so the information of the wireless channel is given by the amplitude and the phase of the estimated CSI. In this sense, although the amplitude can be used directly as a source of information, the phase must be previously corrected since it contains offsets in time and frequency. On the other hand, even having the phase corrected and all the CSI well estimated, algorithms capable of extracting the information and performing the classification or regression are needed. Deep Learning (DL) comes in, which is the other support for CSI-based systems.

While HAR is the application and CSI is the data, DL is the tool capable of analyzing CSI and making the necessary predictions and classifications. The DL model used in each work determines the results obtained and the inputs with which the model works. In many papers, the data fed into the DL model have been previously processed in different ways, and the model inputs are often features extracted from the CSIs rather than from the CSIs themselves. It can be said that the output quality depends on the relationship between the DL model and the data used as inputs to the model. Typically and in most cases, Convolutional Neural Network (CNN) is used, followed by Fully-connected Networks (FC). These networks work very well with data in matrix format, so features are extracted from the CSI and grouped in matrices. On the other hand, Long-Short-Term Memory (LSTM) networks were designed to extract information from time series by means of a "memory mechanism". The mixture of both networks in a CNN-LSTM scheme, called Long-Term Recurrent Convolutional Networks (LRCN) was proposed in [20] and has been employed in recent works, obtaining good results.

WiFi signals and, consequently, collected CSIs are highly sensitive to the environments (i.e., variety of indoor locations and walls between transmitter and receiver), operation conditions (i.e., antenna patterns and SNR), and finally, the surrounding moving people varying in size, shapes or habits. In this context, the term "domain" refers to any aforementioned factor that can cause significant changes over the measured CSI. Based on this, cross-domain implies that a model trained with data from a particular environment, on a particular day and under particular conditions, is able to classify correctly when inputting data from another environment under other conditions. In HAR, the choice of the model is determined by the ability to work under cross-domain conditions [21]. Some DL strategies have this objective, and one of the most prolific is Few-shot Learning (FSL). FSL allows cross-domain adaptation for a few labeled samples from one dataset using a pre-trained model with an extensive dataset. One of the most popular techniques in FSL is the Prototype Networks (PN) [22]. PN is a FSL model based on learning an embedding function to construct an embedding space where the embedding representation of samples from the same class are clustered around a prototype, and those from different classes are separated. Based on PN, few authors have developed Prototypical Recurrent Convolutional Networks (PRCNs) using LRCN as the embedding function [23, 24] to improve the model capacity for temporal events.

Despite the fact that FSL models need few labeled samples of the new domain to perform well, the process of labeling in a new domain is not usually feasible. In this sense, zero-shot learning (ZSL) [25, 26] can deal with this issue. Based on a training domain where a prototype-based metalearner learns to learn, the idea of this paper is to use that domain as a source to create the prototypes for the target domain without labeling new data. In this context, we have developed a zero-shot strategy for our Zero-shot Prototypical Recurrent Convolutional Network (ZPRCN), which allows the generation of prototypes for each class using a CNN-LSTM-FC scheme as embedding function. In contrast to predecessor methods, ZPRCN does not need any labeled samples in the target dataset but creates the prototypes from an available source dataset to directly classify the samples of each new unlabeled and unseen dataset without retraining steps. In this sense, the main contributions of this paper are the following:

- This work proposes a novel prototypical network named ZPRCN in the wireless HAR field. The embedding function of the prototypical network is based on a CNN followed by a LSTM with a FC structure.
- A zero-shot strategy is proposed employing the training dataset to generate the prototypes for a new target domain. This allows ZPRCN to classify correctly new unseen and unlabeled datasets containing the same or similar classes.

- A new measurement campaign has been carried out to evaluate the method extensively. This dataset contains 70 real measurements (i.e., domains) with four human activities varying people, location, day, and reception conditions.
- The proposed model has been evaluated with the new dataset and two other relevant and published datasets [27, 13], all containing similar human activities. As a novelty, an inter-dataset evaluation has been performed, where zero-shot prototypes have been created from a training dataset and another one has been used for testing. To the best of our knowledge, we are the first to do an inter-dataset evaluation in CSI-based systems for HAR.

2 Related Work

This section focuses on previous work on CSI HAR using Deep Learning algorithms. Moreover, other studies using a model similar to the one proposed in this paper are commented on.

The current state of the wireless HAR field is mainly focused on overcoming the difficulties of cross-domain between training data and data collected in other environments [21], as the ability to classify on a single dataset is well studied. In this sense, previous CSI HAR works focus mainly on one type of study: measurements of the same human activities in different scenarios, data pre-processing, and a neural network model application. Other CSI data studies must be considered, like indoor location or crowd counting. Essential papers, in our opinion, are described as follows.

Souvik et al. [28] explore how channel frequency response can be used for an indoor location task, including a linear CSI phase correction to use the phase information together with the amplitude in a posteriori data processing. Wang et al. [4] takes up the same linear phase calibration to use the CSI phase as input in a deep network with three hidden layers and employs the weights of the deep network to represent fingerprints for an indoor location task. In [29], Cheng et al. develop a bi-directional LSTM model for HAR using CSI amplitude. Bahadori et al. [13] study a pre-processing method based on singular value decomposition and linear correlation using CSI amplitude in a PN. The evaluation method implies cross-domain for human activity in three different scenarios, using different antenna numbers. Following this method, Díaz et al. [30] use it to validate a CSI phase processing method for wireless HAR, improving the cross-domain results using the CSI phase. Wang et al. [31] use CSI amplitude in a PN to recognize people and classify them as intruders with a few-sampled dataset. In [32], Zhang et al. propose a CSI-based cross-domain gesture recognition system to achieve comparable recognition accuracy using a dual-path PN, where the added path can be seen as a flexible cluster maker in the embedding space. In [27], Meneghello et al. use the Doppler shift in a novel phase sanitization method and employ a CNN combining data from different antennas to classify activities in a FSL cross-domain evaluation between three scenarios and different configurations.

Some CSI works have proved the use of CNN-LSTM instead CNN in HAR. Wang et al. [33] use a CNN-LSTM deep learning-based framework that integrates the hidden features from both temporal and spatial dimensions from CSI amplitude data profiling activity features from multiple spatial dimensions, and proves the model over five different antenna locations in the same room. Shang et al. [34] change the order and demonstrate that LSTM-CNN outperforms existing models in multi-activity classification. Other works with no CSI data but in HAR field have used this scheme with excellent results. Ordóñez and Roggen [35] propose DeepConvLSTM combining CNNs and LSTMs and applying them to wearable activity recognition. Donahue et al. in [20] propose Long-Term Recurrent Convolutional Networks, combining CNNs and LSTMs and applying them to visual recognition.

For its part, PRCNs have been previously used in some works. In [23], authors employ a scheme CNN-FC-BiLSTM as an embedding function to extract features from X-band SAR images in the MSTAR dataset. In [24], authors use a one-dimensional convolutional layer and two Bi-GRU units as embedding functions to classify speech imagery data, being gated recurrent units (GRUs), a previous and straightforward model of which LSTM units are an evolved stage.

The cross-domain in the previous works assumes few samples labeled in the target domain. Regarding zero-shot learning in CSI-based systems for HAR, Tamzeed et al. [36] propose a system to exploit attributes and context-aware representation of English words with CSI data to recognize new classes. Zhang et al. [37] developed a cross-domain CSI gesture recognition explain a novel param called Body Velocity Profile that is only related to the characteristics of the gesture and removes domain features in Doppler frequency shift. The paper incorporates a "one-fits-all" model that can "train once, use anywhere", which is the same idea behind our work. More recently, Lee et al. [38] studied zero-shot domain adaptation generating "pseudo-labels" in the target domain with a pre-trained model and then using a mixture of labeled samples from the source domain and pseudo-labeled samples from the target domain as support set to re-train the model. Paradigmatically, these three works use models based on LRCN.

Following the application of new models and ZSL, this article explores the use of a PRCN with a novel zero-shot prototype strategy to validate our ZPRCN.

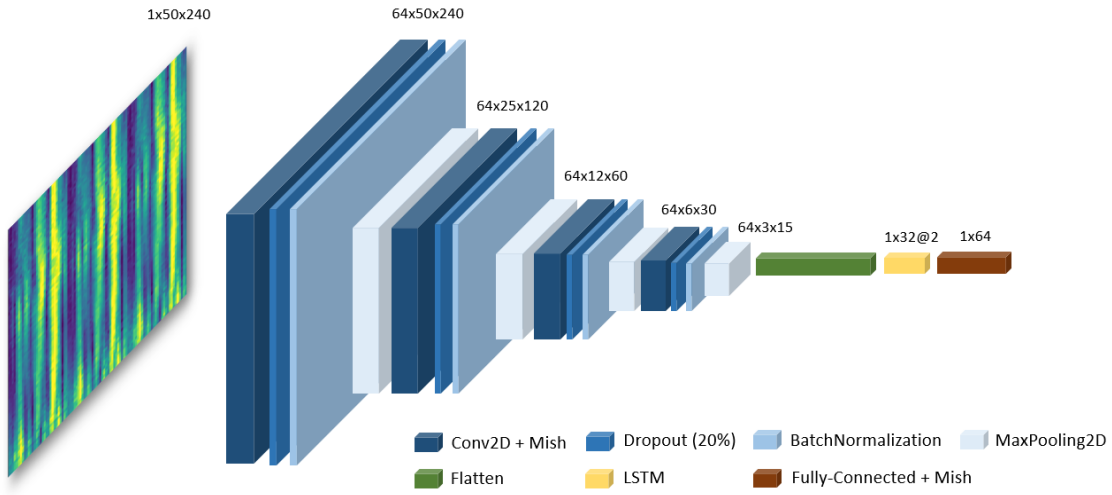

Figure 1: LRCN used as embedding function of the PRCN for this work.

3 Preliminary concepts

3.1 Channel State Information

In OFDM-based technologies, such as WiFi, the received signal in the frequency domain can be modeled as

$$\boldsymbol{y} = \boldsymbol{H} \cdot \boldsymbol{x} + \boldsymbol{z} \tag{1}$$

where $\boldsymbol{y}$ and $\boldsymbol{x}$ denote the received and transmitted signal vectors, respectively, $\boldsymbol{z}$ is the additive complex white Gaussian noise, and $\boldsymbol{H}$ represents a diagonal matrix of the CSI. The CSI of the k-th subcarrier during the s-th symbol, $h_{s,k}$, is a complex value as follows:

$$h_{s,k} = |h_{s,k}|\, e^{j\varphi_{s,k}} \tag{2}$$

where $|h_{s,k}|$ and $\varphi_{s,k}$ are the amplitude and the phase, respectively. The CSI is therefore composed of two independent sources of information: amplitude and phase. Most of the HAR works based on CSI data only use the amplitude for two main reasons. On one hand, the amplitude is more robust against errors during the channel estimation process and, on the other hand, the phase usually contains several synchronization offsets in time and frequency whose estimation is a complex task. In order to avoid phase processing and in the usual practice in this field, this work uses only amplitude information.

3.2 Long-term Recurrent Convolutional Networks

The capacity of the convolutional networks to work on classification tasks, mainly using images as inputs, is well known in the bibliography. Their use with CSI data is widely documented. In general, using CNN with CSI data consists of grouping a number S of OFDM symbols with K subcarriers to generate several matrices with the shape $S \times K$. These matrices can contain the information of the channel variations derived from the human activity in the surrounding area of the WiFi communication during the time interval needed to transmit S OFDM symbols. These matrices can be used in raw as CNN inputs, although signal processing and feature extraction methods are employed in several works.

Conversely, LSTM was developed as part of Recurrent Neural Networks to solve the gradient fading problem. This problem occurs during training using the backpropagation method to update the network weights. In backpropagation, the gradients of the loss function are computed and propagated backward through the network from the last layer to the first layer. The weights are updated in proportion to these gradients. However, as these gradients propagate backward, they can become extremely small, especially in deep networks with many layers. When this happens, the updates of the weights of the lower layers (closest to the input) can be so minor that they are practically zero. As a result, these lower layers learn very slowly, if they learn at all. LSTMs help solve this problem with their particular cell structure, which includes ”gates” to regulate the amount of information stored, forgotten, or transmitted to the next LSTM cell

[39]. This structure makes LSTM an excellent model to work with temporal events, in which information varies temporally. In our case, the channel variations during the activity performance in both time and frequency domains, invite us to prove LSTM cells in a CNN-LSTM scheme for CSI data.

The CNN-LSTM scheme (LRCN) was used for the first time in [20] as a feature extractor for video-based activity recognition. This paper demonstrates that an LRCN feed with 16 frame packets as inputs highly improves the previously employed CNN single frame baseline method for this task, using LSTM cell capacity to learn to recognize and synthesize temporal dynamics for tasks involving sequential data [39]. Since then, LRCN has become a popular model in many fields, mainly where CNNs have obtained good results previously and involve non-stationary events.

3.3 Prototype Networks

The Prototypical Networks idea is to learn an embedding function to construct an embedding space where the embedding representation of samples from the same class are clustered around a prototype, and those from different classes are separated. Given a support set of few labeled samples in the target domain, prototypes of each class are generated with the embedded support points. Classification is then performed for the embedded points of a query set of unlabeled samples by finding the nearest class prototype in the embedding space. The class prototype is taken as the mean of the support points in the embedding space, and Euclidean distance is used as distance function in the embedding space.

In zero-shot prototype networks, some kind of class meta-data is used to determine the prototypes, so that meta-data and query samples come from different domains.

4 Cross-domain strategy with Prototypical Networks

4.1 Model

Let $\mathcal{S} = \{(\boldsymbol{x}_1, y_1), (\boldsymbol{x}_2, y_2), \ldots, (\boldsymbol{x}_N, y_N)\}$ be a set of labeled samples where each $\boldsymbol{x}_i \in \mathbb{R}^{SK}$ is the SK-dimensional feature vector of S time-windowed CSIs and $y_i \in \{1, \ldots, C\}$ is the corresponding label. A prototypical network maps input data into an M-dimensional embedding space through an embedding function $f : \mathbb{R}^{SK} \rightarrow \mathbb{R}^M$ related with a DL model. In few-shot classification, each prototype is the mean vector of the embedded points of a support set $\mathcal{S}_k$ belonging to a certain class $k \in \{1, \ldots, C\}$ such that

$$\boldsymbol{c}_k = \frac{1}{|\mathcal{S}_k|} \sum_{(\boldsymbol{x}_i, y_i) \in \mathcal{S}_k} f(\boldsymbol{x}_i) \tag{3}$$

where $|\mathcal{S}_k|$ is the cardinality of the support set $\mathcal{S}_k$.

The proposed architecture associated to the embedding function f is the LRCN model shown in Fig. 1. Therefore, the PRCN is a mixture of a standard PN and a LRCN, and could be defined as a kind of improved PN for temporal events. The idea is to replace the CNN for a LRCN to generate the embedding space, taking advantage of LSTM cell capacity to remember functional information in events with temporal evolution. The LRCN comprises four consecutive convolutional blocks, a vectorization layer, two LSTM cells, and finally, a fully-connected layer.

Each convolutional block consists of one 2D-convolutional layer, one dropout layer (20%), one batchnormalization layer, and a final 2D max-pooling layer. The convolutional layer extracts features from the input image (or on the previous layer's output in deeper blocks of the network). The dropout layer shuts down specific neurons at each training iteration, and is used to avoid overfitting the network to the incoming data and improve generalization capability. The normalization layer normalizes the data by adjusting its mean and variance to the same values for each input batch, and the final max-pooling layer is used to reduce the dimensionality of each block's output and reduce the output's dimensions while preserving the dominant features.

As mentioned above, the LSTM layers handle the long-term dependencies in the sequential data. In our LRCN, we employ a typical configuration of two consecutive layers, which generate a 32-dimensional vector as output. Finally, the fully-connected layer adds an extra layer of non-linear processing, aids in transforming the sequential information into a fixed set of features, and generates a 64-dimensional space.

4.2 Zero-shot learning

The use of the term zero-shot learning in the context of cross-domain CSI is appropriate when dealing with situations where the model must make inferences in a target domain without having been previously exposed to labeled data specific to that domain. Several works in the literature use it even if both domains have the same classes since the

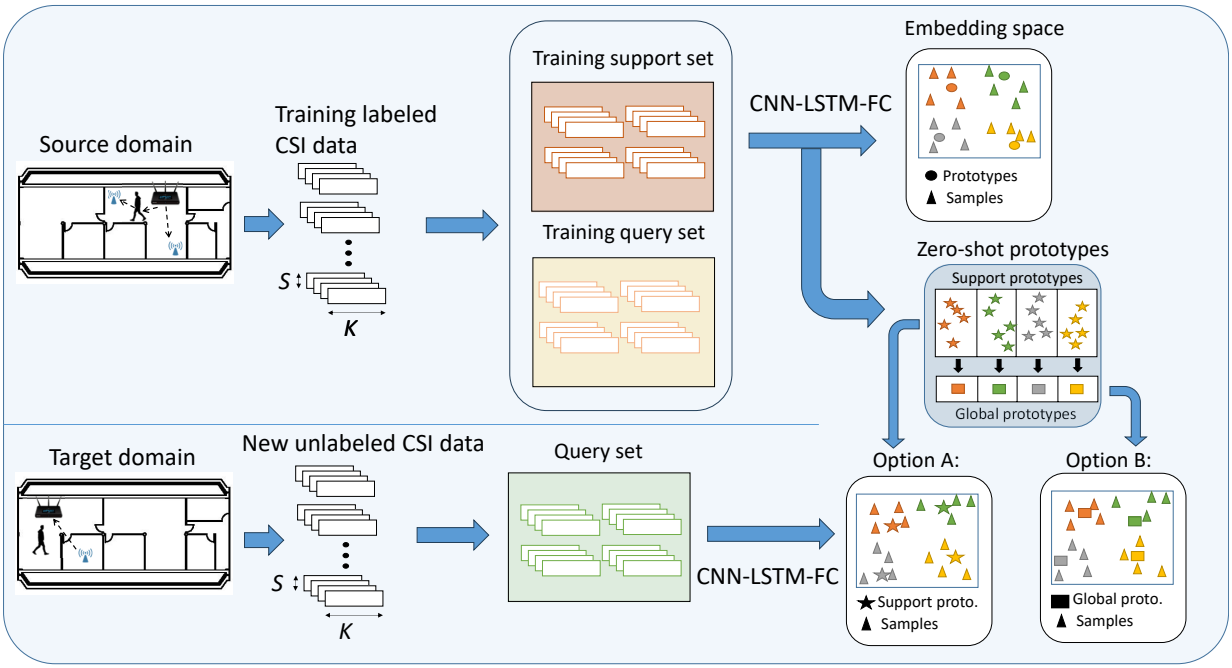

Figure 2: Zero-shot strategies for cross-domain activity recognition. Prototypes are computed from CSIs of the source domain (option A uses support prototypes and option B global prototypes) and new unlabeled samples of a similar activity are taken from CSIs of the target domain, which location, WiFi device positions and measurement scenario differ from the source domain.

samples belong to different domains. In this section, we explain the zero-shot strategy based on cross-domain datasets that contain the same (intra-dataset) or similar (inter-datasets) classes.

As section 3.3 mentions, PN divides data into two subsets: the labeled support set and the unlabeled query set. The support set is used to generate a prototype of each class by averaging the samples of that class using (3). Once the prototypes are generated, the Euclidean distance from each sample of the query set to each class prototype is measured. Therefore, assuming a query set of unlabeled samples $\mathcal{Q} = \{\boldsymbol{x}_1, \boldsymbol{x}_2, \ldots, \boldsymbol{x}_Q\}$, classification for a given sample $\boldsymbol{x}_i$ is carried out by finding the minimum distance to the prototypes as follows

$$\hat{y}_i = \arg \min_{j \in \{1,\ldots,C\}} ||\boldsymbol{x}_i - \boldsymbol{c}_j||^2 \tag{4}$$

where $\hat{y}_i$ is the estimated class for the sample $\boldsymbol{x}_i$.

4.2.1 Support prototypes from the source domain

Considering cross-domain training and target datasets that include similar human activities, FSL in HAR is usually carried out when few labeled samples of each class in the target dataset are available. In this work, a zero-shot strategy is proposed assuming available the labeled samples of a training dataset as meta-data for the generation of the embedded prototypes to classify samples from another unlabeled and not seen previously dataset. Therefore, considering a training labeled dataset $\mathcal{S}$ as previously defined and a new unlabeled dataset $\mathcal{T}$ obtained from a new target domain, so that both datasets contain same classes, the proposed zero-shot strategy uses labeled samples from $\mathcal{S}$ to generate the prototypes as in (3) from a support set $\mathcal{S}_k$ for each class k. Afterward, classification of an unlabeled sample $\boldsymbol{s}_i \in \mathcal{T}$ is carried out as follows

$$\hat{y}_i = \arg \min_{j \in \{1,\ldots,C\}} ||\boldsymbol{s}_i - \boldsymbol{c}_j||^2. \tag{5}$$

The proposed scheme is depicted in the option A of Fig. 2, where one can observe that the prototypes are obtained from a labeled dataset of a source domain and utilized for classification of new samples of other target domain.

4.2.2 Global prototypes from the source domain

A different method, called Global Prototypes (GP), is proposed to generate the global prototype for each class by averaging all the support prototypes for that class obtained from the training dataset $\mathcal{S}$ of the source domain. This allows us to save the global prototypes of each class directly and load them when using a new dataset. For a sufficiently large number of support prototypes in the source domain, this strategy is equivalent to calculating a prototype as in (3) with a support set $\mathcal{S}_k$ containing all samples of the class k. As shown in option B of the Fig. 2, the trained embedding function and the global prototypes obtained from the source domain are shared to classify in the target domain. Both proposed methods are analyzed in the results section.

5 Datasets

This section explains the three datasets (named A, B, and C) of WiFi CSIs, which have been used to test the proposed methods. These datasets include the channel measurements provided by various WiFi devices for different human activities and indoor environments. All datasets include the following actions (i.e., classes): empty, jump, walk, stand. Dataset A is a new dataset of a measurement campaign carried out in our facilities; the new dataset is not published yet, but it is accessible upon request. Datasets B and C are public, and their characteristics are described in detail in [40] and [13], respectively.

5.1 Dataset A

This dataset contains CSI data related to activity recognition recorded in the facilities of the Bilbao School of Engineering at the Univesity of the Basque Country (UPV/EHU). The measures have been taken in three different scenarios. The first scenario is located in the basement, isolated from other WiFi signals. The map of this location is shown in Fig. 3 (up). The recordings were made over two non-consecutive days, changing the transmitter's position to change the propagation channels and simulate two different environments. The communication between the TX and RXs is performed with the transmission of a large file via FTP. The second and third scenarios are a laboratory and a storage room shown in Fig. 3 (down). They are located side by side on the sixth floor of the building, and the communication between the TX and RXs is given using an iPerf3 test, which creates traffic to measure the network performance. The recordings were made on the same day, three months later than the basement measurements.

For the activity recognition, four men and one woman, aged 32 to 60, participated in the activities, and each person performed each activity alone in the room for one minute. Participants perform the following activities: jumping, standing, walking, and an empty class. The activities are performed consecutively, with a thirty-second rest period between them. Participants receive no instructions or guidelines on performing the activity to simulate a situation as naturally as possible. The activities are always performed at or around the same point, marked with a person icon in Fig. 3.

In total, this dataset contains 70 one-minute-long measurements (i.e., 70 different domains). Therefore, the measurement named Ss-RXr-Pp corresponds to the recorded CSIs with a person, p, using a Raspberry, r, in a scenario, s. For example, the measurement in the laboratory of person 1 using RX3 is called S3P1RX3, while the same measurement in the basement on the first day is called S1P1RX3. In Table 1, details of the four scenarios are given. That is, the location of the measurements, number of RXs to collect data, the day of the measurement, and the data transmission protocol between WiFi devices. To report the results comprehensively, we have selected four training subsets; concretely, we have selected S1RX1P1, S2RX2P2, S3RX3P3, and S4RX4P4, in order to cover different scenarios, receivers and people.

Table 1: Details of the scenarios for CSI data acquisition of Dataset A.

Scenario	Location	Day	RXs	TX Protocol
S1	Basement	1	3	FTP
S2	Basement	2	3	FTP
S3	Laboratory	1	4	iPerf3
S4	Storage room	1	4	iPerf3

The dataset has been recorded using Raspberrys Pi and the Nexmon CSI Tool software [41] to extract the CSI data. It contains three scenarios in which three or four Raspberries are in listening mode and are used as receivers (RXs). Ethernet cables connect these Raspberrys to the same router that sends the information from Raspberries to a laptop. The CSIs were calculated at a rate of 1 kHz, in the 5 GHz band, for a bandwidth (BW) of 80 MHz, with 256 subcarriers. However, after eliminating guard, pilot, and empty subcarriers, the final number of subcarriers is K = 240. In this

sense, each RX picks up a different number of frames due to different distances to the TX, the direction of each antenna, human activity, and elements in the room, however, it is a balanced dataset in which all classes has a similar number of frames as shown in Table 2 for the selected training sets.

Table 2: Number of samples of size 50×240 of each class for each training set in Dataset A.

Class	S1RX1P1	S2RX2P2	S3RX3P3	S4RX4P4
Empty	1256	637	1375	1434
Stand	1264	715	1388	1420
Walk	1292	368	1369	1428
Jump	1230	356	1366	1393

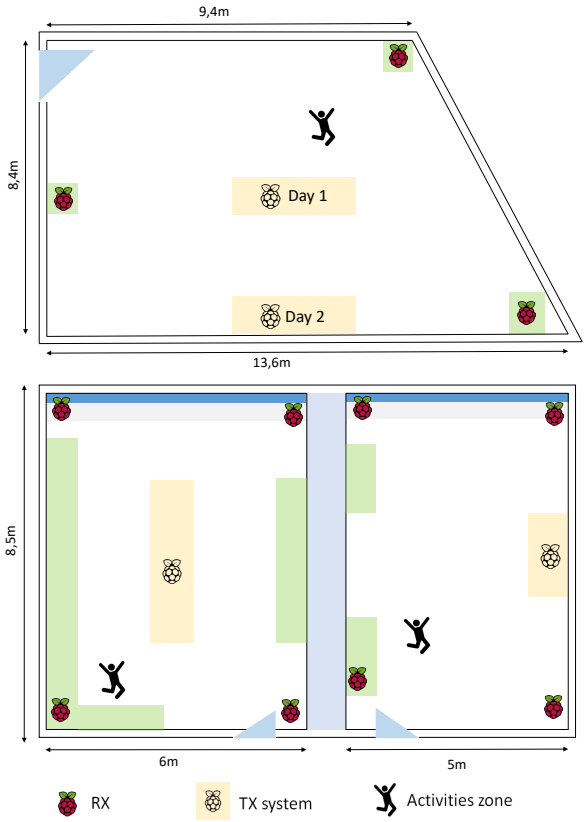

Figure 3: Rooms for experimental measurements used in Dataset A: Basement (up), laboratory (down left) and storage room (down right).

5.2 Dataset B

This dataset, published in [40], contains measurements for seven people who performed seven activities in seven different environments. Out of the seven activities, four are used in this paper: empty, walking, jumping and standing. Data from these activities were collected using a monitoring router and the Nexmon CSI tool, which estimates the channel frequency response of ongoing Wi-Fi transmissions. The monitored traffic was generated by an IEEE 802.11ac-enabled Wi-Fi router transmitting data to a receiving device in the 5 GHz band, using an 80 MHz BW, a bitrate of 173 packets per second, and with $K = 242$ subcarriers.

The total measured scenarios for activity recognition are nine in five different campaigns. However, only six scenarios contain the classes that this work analyzes, so we have selected six scenarios: AR-1, AR-2, AR-3, AR-4, AR-5 and AR-7, all from the campaign named a in [40]. In Table 3, the amount of samples for each class is provided. As in Dataset A, each sample is a matrix with $S = 50$ consecutive CSIs and $K = 240$ subcarriers. The number of samples provided for each location and class is given in Table 3.

Table 3: Number of samples of size 50×240 of each class for each subset in Dataset B.

Class	AR-1	AR-2	AR-3	AR-4	AR-5	AR-7
Empty	1592	1730	1687	1665	1615	1598
Stand	1654	1603	1628	1621	1659	1634
Walk	1676	1682	1617	1666	1632	1639
Jump	1644	1656	1619	1678	1662	1628

5.3 Dataset C

The authors in [13] carried out these measurements in three different scenarios. The experiments involved two subjects who were given instructions on the type, duration, and location of activities such as jumping, walking, and standing. Each measurement campaign involved 180 seconds of data collection for each activity performed by the two people. Measurements were repeated ten times with a time interval of at least 2 hours between measurements. Dataset C performs CSI measurements in three environments: an office area $E1$, a meeting room $E2$, and a classroom $E3$, on different days and times.

For the generation of the dataset, the authors used three Asus RT-AC86U WiFi routers, each equipped with four antennas. The routers extracted the CSI packets using the Nexmon firmware [41]. The CSIs were calculated at a rate of 100 Hz, in the 5 GHz band, for 20 and 80 MHz BW, with K = 52 and K = 242 subcarriers, respectively. The number of samples provided for each location and class is given in Table 4.

Table 4: Number of 50×240-sized samples of each class for each scenario in Dataset C.

Class	E1	E2	E3
Empty	331	264	275
Stand	246	124	186
Walk	339	331	337
Jump	332	332	327

6 Results and discussion

This section reports the obtained results with the three datasets. First, a standard PN[2] and the proposed ZPRCN model have been compared. Afterward, a performance evaluation of the ZPRCN is carried out with different domains in the Dataset A. Finally, one inter-datasets assessment shows the performance results of the model being trained in one dataset and directly tested in another extracting the prototypes from training dataset. As shown in Tables 2, 3 and 4, the three datasets are balanced in terms of samples per class. Therefore, accuracy has been used as a performance metric to evaluate the model. The input data of the ZPRCN model are 50×240-sized matrices of the amplitudes of the CSIs without additional preprocessing. The main params for training are shown in Table 5.

Table 5: Training params

Params	Value
Input shape	(1, 50, 240)
Learning rate (fixed)	0.001
Classes number	4
Support set size	4
Query set size	4
Epochs	2
Epoch size	500

6.1 Comparison of the standard PN and ZPRCN

First, to illustrate the clusterization capacity of ZPRCN vs. PN, a typical high dimensional data visualization method, i.e. t-distributed stochastic neighbor embedding (t-SNE)[42], is utilized to visualize the embedding vectors. In this sense, the Fig.4 represents the t-SNE distribution for each class in both models. Each sample represents one class

[2]For this work, PN uses the same CNN architecture depicted in Fig. 1 without LSTM and FC layers.

Table 6: Comparison between the accuracy obtained by ZPRCN vs. a standard PN, employing the Support Prototypes strategy. Accuracy values are the average of all RX.

Test	**Train**							
	S1RX1P1		S2RX2P2		S3RX3P3		S4RX4P4	
	ZPRCN	*PN*	*ZPRCN*	*PN*	*ZPRCN*	*PN*	*ZPRCN*	*PN*
S1P1	1	0.23	1	0.34	0.97	0.49	0.99	0.28
S1P2	1	0.32	1	0.27	0.97	0.22	0.99	0.51
S1P3	1	0.30	1	0.37	0.98	0.26	1	0.31
S1P4	1	0.22	1	0.24	0.98	0.31	0.99	0.35
S1P5	1	0.27	1	0.41	0.98	0.29	0.98	0.29
S2P1	1	0.43	1	0.39	0.95	0.25	0.94	0.36
S2P2	1	0.50	1	0.23	0.96	0.31	0.95	0.32
S2P3	1	0.36	1	0.22	0.95	0.24	0.95	0.33
S2P4	1	0.22	1	0.23	0.96	0.35	0.95	0.33
S2P5	1	0.27	1	0.32	0.95	0.33	0.95	0.34
S3P1	1	0.23	1	0.36	0.97	0.29	0.99	0.44
S3P2	1	0.25	1	0.29	0.97	0.36	0.99	0.29
S3P3	1	0.32	1	0.23	0.98	0.42	0.98	0.22
S3P4	1	0.47	1	0.52	0.98	0.28	0.98	0.36
S3P5	1	0.25	1	0.31	0.97	0.29	0.97	0.50
S4P1	1	0.32	1	0.30	0.99	0.22	0.99	0.26
S4P2	1	0.35	1	0.33	0.99	0.23	0.99	0.32
S4P3	1	0.43	1	0.27	0.99	0.27	0.99	0.23
S4P4	1	0.31	1	0.30	0.99	0.51	0.98	0.42
S4P5	1	0.31	1	0.48	0.99	0.39	0.97	0.38

prototype in each of the 500 iterations for the second epoch in the training. It can be seen that the use of ZPRCN visibly improves the clustering of the prototypes in each class since time-related features from the time-windowed CSI matrix can be exploited through the LSTM in order to create the embedding function f of the ZPRCN.

Table 6 shows the accuracies for the classification task using PN and ZPRCN with the zero-shot Support Prototypes strategy. Accuracies have been averaged for all RX and all activities in a given scenario with a certain person. Whereas the results of the PN network occasionally exceed 50% accuracy, the ZPRCN network shows a high classification capability of close to 100% in all cases. Therefore, results demonstrate that the proposed ZPRCN network far exceeds the HAR capabilities of a standard PN network in cross-domain sensing.

6.2 Assessment of zero-shot strategies over Dataset A

In this section, an extensive evaluation of the proposed strategies is performed for the Dataset A. As indicated in section 5.1, we have selected S1RX1P1, S2RX2P2, S3RX3P3 and S4RX4P4 subsets as training sets for clarity in the results presentation covering a variety of scenarios, receivers and people.

Table 7 shows the accuracies of the model, training with each selected training subset and tested in all measurements, which include all combinations of scenarios, people and receivers, and using both Support Prototypes (SP) and Global Prototypes (GP) strategies. To facilitate the visualization of the results, different colors indicate a range of accuracy

(a) PN (b) PRCN

Figure 4: t-SNE distribution for prototypes of each class generated among 500 iterations, for standad PN and the ZPRCN. Data from S1RX1P1 subset in Dataset A.

values: black for accuracies in the (0.95, 1] interval, green for accuracies in the (0.9, 0.95] range, blue for values in (0.8, 0.9] and red for accuracies smaller and equal to 0.8.

The results presented in Table 7 reveal the high ability of the PRCN model to distinguish each of the four selected classes (empty, stand, jump, walk) independently of the changes in the measurement domain, such as different scenarios, different people, different receivers in each measure, and even to data transfer using FTP or iPerf3 protocol. For example, SP strategy training with S1P1RX1 and S2P2RX2 obtains a 100% accuracy in each of the 70 measurements, and the same for GP strategy training with S3P3RX3. In the other training subsets, accuracies are also nearly 100%, with a few exceptions. Only the GP strategy trained with S2P2RX2 subset has accuracy values smaller than 80% for 10 out of 70 testing subsets.

To add information about each class classification, Figures 5 and 6 show the confusion matrices for the four training subsets evaluated in the 70 measured configurations for the SP and GP strategies, respectively. Again, the high accuracy obtained for each class in both strategies is remarkable. For the SP strategy, the minimum accuracy obtained has been 0.98, with an average of one or close to one in the four cases. GP strategy has also obtained good results. Lower values have been achieved for S1P1RX1 in *stand* and *walk* classes. In contrast, classification of 100% is reached for S3P3RX3.

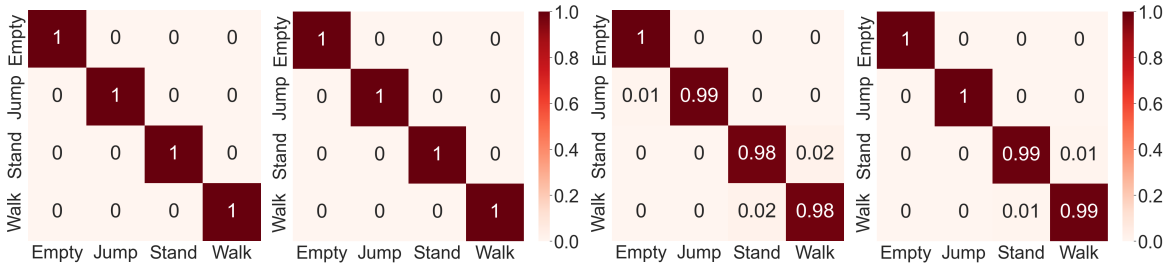

(a) S1RX1P1 (b) S2RX2P2 (c) S3RX3P3 (d) S4RX4P5

Figure 5: Support Prototypes strategy in Dataset A: Confusion matrices for each training subset. Accuracies are the average of all of 70 testing subsets.

.

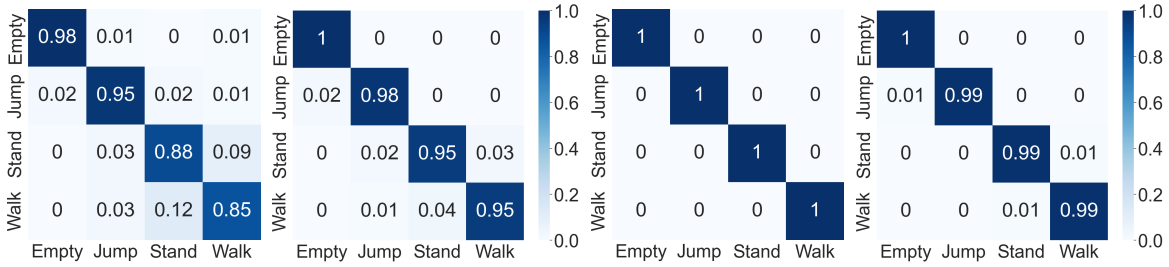

(a) S1RX1P1 (b) S2RX2P2 (c) S3RX3P3 (d) S4RX4P5

Figure 6: Global Prototypes strategy in Dataset A: Confusion matrices for each training subset. Accuracies are the average of all 70 testing subsets.

.

In general, we can observe a very high performance of the proposal during the evaluation in Dataset A, with a slightly higher precision for the SP strategy in some cases; however, it does not seem decisive to choose one. In addition, it is worth-noticing that the proposed ZPRCN offers an excellent classification performance for zero-shot strategies in cross-domain HAR scenarios with similar activities.

6.3 Inter-dataset evaluation

In order to evaluate the robustness of the proposal with other datasets from the literature, an inter-datasets evaluation has been implemented. This evaluation method follows the same procedure of the previous subsections, consisting of training the ZPRCN with one dataset and directly testing the trained model in another. Prototypes are generated from the training datasets as shown in Fig. 2, following the SP and GP strategies. The parameters of the training process maintain the values of Table 5.

Table 7: Accuracy values for Dataset A employing the SP and GP strategies with our ZPRCN. Colors indicate accuracy range: black for acc ∈ (0.95, 1], green for acc ∈ (0.9, 0.95], blue for acc ∈ (0.8, 0.9] and red for acc ⩽ 0.8.

	Train							
Test	S1RX1P1		S2RX2P2		S3RX3P3		S4RX4P4	
	SP	GP	SP	GP	SP	GP	SP	GP
S1RX1P1	1.00	1.00	1.00	0.96	1.00	1.00	0.99	1.00
S1RX1P2	1.00	1.00	1.00	0.97	1.00	1.00	0.99	1.00
S1RX1P3	1.00	1.00	1.00	0.98	1.00	1.00	1.00	0.97
S1RX1P4	1.00	1.00	1.00	0.97	1.00	1.00	1.00	0.94
S1RX1P5	1.00	1.00	1.00	0.99	1.00	1.00	0.94	0.95
S1RX2P1	1.00	0.75	1.00	1.00	0.90	1.00	1.00	1.00
S1RX2P2	1.00	0.80	1.00	1.00	0.93	1.00	1.00	1.00
S1RX2P3	1.00	0.94	1.00	1.00	0.95	1.00	1.00	1.00
S1RX2P4	1.00	0.92	1.00	1.00	0.95	1.00	1.00	1.00
S1RX2P5	1.00	0.80	1.00	1.00	0.94	1.00	1.00	1.00
S1RX3P1	1.00	1.00	1.00	0.93	1.00	1.00	1.00	1.00
S1RX3P2	1.00	1.00	1.00	0.93	1.00	1.00	1.00	0.96
S1RX3P3	1.00	1.00	1.00	0.94	1.00	1.00	1.00	1.00
S1RX3P4	1.00	1.00	1.00	0.93	1.00	1.00	1.00	0.98
S1RX3P5	1.00	1.00	1.00	0.94	1.00	1.00	1.00	1.00
S2RX1P1	1.00	0.77	1.00	1.00	0.98	1.00	1.00	0.99
S2RX1P2	1.00	0.78	1.00	1.00	0.99	1.00	1.00	1.00
S2RX1P3	1.00	0.92	1.00	1.00	0.97	1.00	1.00	0.98
S2RX1P4	1.00	0.92	1.00	1.00	0.98	1.00	1.00	0.98
S2RX1P5	1.00	0.89	1.00	1.00	0.97	1.00	1.00	0.98
S2RX2P1	1.00	1.00	1.00	0.95	1.00	1.00	0.88	0.95
S2RX2P2	1.00	1.00	1.00	0.96	1.00	1.00	0.88	0.94
S2RX2P3	1.00	0.98	1.00	0.92	1.00	1.00	0.88	0.94
S2RX2P4	1.00	0.97	1.00	0.94	1.00	1.00	0.88	0.92
S2RX2P5	1.00	0.95	1.00	0.94	1.00	1.00	0.88	0.91
S2RX3P1	1.00	0.80	1.00	0.87	0.89	1.00	0.95	1.00
S2RX3P2	1.00	0.77	1.00	0.84	0.90	1.00	0.97	1.00
S2RX3P3	1.00	0.77	1.00	0.84	0.88	1.00	0.97	0.95
S2RX3P4	1.00	0.78	1.00	0.86	0.91	1.00	0.98	1.00
S2RX3P5	1.00	0.76	1.00	0.86	0.89	1.00	0.96	0.91
S3RX1P1	1.00	0.95	1.00	0.97	1.00	1.00	1.00	1.00
S3RX1P2	1.00	0.97	1.00	0.90	1.00	1.00	1.00	1.00
S3RX1P3	1.00	0.99	1.00	0.90	1.00	1.00	1.00	1.00
S3RX1P4	1.00	0.97	1.00	0.94	0.99	1.00	1.00	1.00
S3RX1P5	1.00	0.98	1.00	1.00	0.99	1.00	1.00	1.00
S3RX2P1	1.00	0.90	1.00	1.00	0.91	1.00	1.00	1.00
S3RX2P2	1.00	0.90	1.00	1.00	0.89	1.00	1.00	1.00
S3RX2P3	1.00	0.95	1.00	1.00	0.95	1.00	1.00	1.00
S3RX2P4	1.00	0.93	1.00	1.00	0.94	1.00	1.00	1.00
S3RX2P5	1.00	0.94	1.00	1.00	0.93	1.00	1.00	1.00
S3RX3P1	1.00	0.97	1.00	0.99	1.00	1.00	0.99	0.89
S3RX3P2	1.00	0.94	1.00	0.99	1.00	1.00	0.99	0.96
S3RX3P3	1.00	0.88	1.00	0.94	1.00	1.00	0.94	0.92
S3RX3P4	1.00	0.93	1.00	0.93	1.00	1.00	0.93	0.87
S3RX3P5	1.00	0.94	1.00	0.98	1.00	1.00	0.92	0.86
S3RX4P1	1.00	0.95	1.00	1.00	1.00	1.00	0.98	0.88
S3RX4P2	1.00	0.94	1.00	1.00	1.00	1.00	0.98	0.93
S3RX4P3	1.00	0.94	1.00	1.00	1.00	1.00	0.98	0.97
S3RX4P4	1.00	0.94	1.00	1.00	1.00	1.00	0.98	0.95
S3RX4P5	1.00	0.94	1.00	1.00	1.00	1.00	0.97	0.91
S4RX1P1	1.00	0.93	1.00	0.91	1.00	1.00	1.00	0.97
S4RX1P2	1.00	0.90	1.00	0.91	1.00	1.00	1.00	0.96
S4RX1P3	1.00	0.88	1.00	0.91	1.00	1.00	1.00	0.98
S4RX1P4	1.00	0.85	1.00	0.91	1.00	1.00	1.00	0.97
S4RX1P5	1.00	0.86	1.00	0.91	1.00	1.00	1.00	0.96
S4RX2P1	1.00	0.88	1.00	0.98	1.00	1.00	0.99	0.99
S4RX2P2	1.00	1.00	1.00	0.99	1.00	1.00	0.99	0.99
S4RX2P3	1.00	0.99	1.00	0.99	1.00	1.00	0.99	0.99
S4RX2P4	1.00	0.98	1.00	0.99	1.00	1.00	0.99	0.99
S4RX2P5	1.00	0.98	1.00	0.99	1.00	1.00	0.99	0.99
S4RX3P1	1.00	1.00	1.00	1.00	1.00	1.00	1.00	0.97
S4RX3P2	1.00	1.00	1.00	1.00	1.00	1.00	1.00	0.97
S4RX3P3	1.00	1.00	1.00	1.00	1.00	1.00	1.00	0.95
S4RX3P4	1.00	1.00	1.00	1.00	1.00	1.00	1.00	0.95
S4RX3P5	1.00	1.00	1.00	1.00	1.00	1.00	1.00	0.94
S4RX4P1	1.00	0.91	1.00	1.00	1.00	1.00	1.00	1.00
S4RX4P2	1.00	0.90	1.00	1.00	1.00	1.00	1.00	1.00
S4RX4P3	1.00	0.92	1.00	1.00	1.00	1.00	1.00	1.00
S4RX4P4	1.00	0.88	1.00	1.00	1.00	1.00	1.00	1.00
S4RX4P5	1.00	0.85	1.00	1.00	1.00	1.00	1.00	1.00

Tables 8 and 9 report the results obtained training our ZPRCN using the Dataset A and testing in Datasets B and C, respectively. As a first consideration, both tables show results close to a 100% accuracy.

Paying attention to Table 8, results show that the SP strategy has been more effective since for the training subsets S1RX1P1 and S3RX3P3, the accuracies of the GP strategy are significantly lower. It must be taken into account that the subsets of Dataset B are varied; three different scenarios are employed and each measure is taken with different configurations, with direct and obstructed vision between transmitter and receiver, and with different people. In general, SP strategy shows a slightly higher difficulty in classifying for subsets AR-3, AR-4, and AR-5, probably due to a lower quality of the CSIs in difficult reception conditions. In this sense, AR-3 and AR-4 are subsets with an obstructed line of sight between transmitter and receiver, and subset AR-5, measured in a furnished living room, may have been more affected by other considerations relating to the change of environment. However, it should be noted that the model trained with the S2RX2P2 subset was able to overcome these difficulties and obtained 100% accuracy using both SP and GP. Similarly, the model trained with the S3RX3P3 subset using the SP strategy only dropped from 100% to 96% in the AR-3 subset. Furthermore, the results in Table 9 are even better than those achieved in Table 8. These values are all close to 100% accurate, with a greater similarity in assessing both SP and GP strategies. Given these results, it can be stated that the proposed ZPRCN offers significant robustness for zero-shot HAR in cross-domain conditions.

Table 8: Accuracy values for Dataset B using the trained model with Dataset A subsets for Support Prototypes (SP) and Global Prototypes (GP) strategies.

	Dataset A (Train)							
Dataset B	S1RX1P1		S2RX2P2		S3RX3P3		S4RX4P4	
(Test)	SP	GP	SP	GP	SP	GP	SP	GP
AR-1	1	0.79	1	1	1	0.90	1	0.95
AR-2	1	0.81	1	1	1	0.80	1	1
AR-3	0.97	0.82	1	1	0.96	0.86	0.95	0.99
AR-4	0.91	0.80	1	1	1	0.81	0.98	0.92
AR-5	0.95	0.85	1	1	1	0.83	0.92	0.99
AR-7	1	0.78	1	1	1	0.81	1	0.94

Table 9: Accuracy values for Dataset B using the trained model with Dataset A subsets for Support Prototypes (SP) and Global Prototypes (GP) strategies.

	Dataset A (Train)							
Dataset C	S1RX1P1		S2RX2P2		S3RX3P3		S4RX4P4	
(Test)	SP	GP	SP	GP	SP	GP	SP	GP
E1	0.99	1	1	1	1	1	1	0.96
E2	0.98	1	1	1	0.95	1	1	0.95
E3	0.98	0.97	1	0.99	0.98	1	1	0.98

In order to generalize the model further, Table 10 shows the results applying the PRCN over the two public datasets, training with Dataset B and testing on Dataset C. In this case, both strategies give results close to 100% training the model with the subsets AR-1, AR-2, AR-4 and AR-7 and testing on the three environments of Dataset C. The SP strategy also maintains those values for the AR-3 subsets, but obtains lower accuracy values training with the AR-5 subset. The results of the GP strategy are also lower for the AR-3 and AR-5 subsets. In any case, these results confirm the cross-domain effectiveness of the PRCN model proposed in the paper and the SP strategy as the most effective.

7 Conclusion

In this work, the authors present a novel Zero-shot Prototypical Recurrent Convolutional Network (ZPRCN) and two zero-shot strategies to advance solutions to the cross-domain problem using CSI data in HAR domains.

In this sense, the proposed ZPRCN network significantly improves the classification performance of a standard PN network, as can be seen in Fig. 4 and Table 6. The LSTM cell's capacity to find temporal events is critical to relating temporal wireless channel variations with each activity.

In addition, zero-shot strategies offer robust and remarkable results in cross-domain activity recognition. In particular, SP accuracies are close to 100% in most evaluation cases, including the inter-datasets section. The evaluation of the zero-shot strategies has been exhaustive using three different datasets, each of them measured in different scenarios

Table 10: Accuracy values for Dataset C using the trained model with Dataset B subsets for Support Prototypes (SP) and Global Prototypes (GP) strategies. For the best appearance, train and test columns are changed in relation to the other tables.

Dataset B (Train)	**Strategy**	**Dataset C (Test)** E1	E2	E3
AR-1	SP	1	1	1
	GP	1	1	1
AR-2	SP	1	1	1
	GP	1	1	0.99
AR-3	SP	1	1	1
	GP	0.84	1	0.91
AR-4	SP	1	1	1
	GP	0.98	0.97	0.97
AR-5	SP	0.88	0.89	0.88
	GP	0.87	0.87	0.86
AR-7	SP	1	1	1
	GP	1	1	0.98

which change topology, obstacles, furniture, people, days and hardware. The presented results validate the proposal's ability to surpass the current state-of-the-art on cross-domain in wireless HAR using CSI, and open the door to future works even in other disciplines.

8 Acknowledgment

This work has been financially supported by the Basque Government (under grant IT1436-22) and by the Spanish Government (under grant PID2021-124706OB-I00, funded by MCIN/AEI/10.13039/501100011033 and by ERDF A way of making Europe).

References

[1] C. Chen, H. Song, Q. Li, F. Meneghello, F. Restuccia, and C. Cordeiro, "Wi-fi sensing based on ieee 802.11bf," *IEEE Communications Magazine*, vol. 61, no. 1, pp. 121–127, 2023.

[2] I. Sobron, J. D. Ser, I. Eizmendi, and M. Velez, "Device-Free People Counting in IoT Environments: New Insights, Results, and Open Challenges," *IEEE Internet of Things Journal*, vol. 5, pp. 4396–4408, 12 2018.

[3] J. R. M. Bernaola, I. Sobrón, J. Del Ser, I. Landa, I. Eizmendi, and M. Vélez, "Ensemble learning for seated people counting using wifi signals: Performance study and transferability assessment," in *2021 IEEE Globecom Workshops (GC Wkshps)*, 2021, pp. 1–6.

[4] X. Wang, L. Gao, and S. Mao, "CSI Phase Fingerprinting for Indoor Localization with a Deep Learning Approach," *IEEE Internet of Things Journal*, vol. 3, pp. 1113–1123, 12 2016.

[5] K. Qian, C. Wu, Z. Yang, Y. Liu, H. E. Fugui, and T. Xing, "Enabling contactless detection of moving humans with dynamic speeds using CSI," *ACM Transactions on Embedded Computing Systems*, vol. 17, 2 2018.

[6] Y. Xu, W. Yang, J. Wang, X. Zhou, H. Li, and L. Huang, "Wistep: Device-free step counting with wifi signals," *Proc. ACM Interact. Mob. Wearable Ubiquitous Technol.*, vol. 1, no. 4, jan 2018. [Online]. Available: https://doi.org/10.1145/3161415

[7] J. Liu, L. Wang, L. Guo, J. Fang, B. Lu, and W. Zhou, "A research on CSI-based human motion detection in complex scenarios," in *2017 IEEE 19th International Conference on e-Health Networking, Applications and Services (Healthcom)*, 2017, pp. 1–6.

[8] Y. Zeng, D. Wu, R. Gao, T. Gu, and D. Zhang, "FullBreathe: Full Human Respiration Detection Exploiting Complementarity of CSI Phase and Amplitude of WiFi Signals," *Proceedings of the ACM on Interactive, Mobile, Wearable and Ubiquitous Technologies*, vol. 2, pp. 1–19, 9 2018.

[9] Y. Zeng, Z. Liu, D. Wu, J. Liu, J. Zhang, and D. Zhang, "A multi-person respiration monitoring system using cots wifi devices." Association for Computing Machinery, 9 2020, pp. 195–198.

[10] A. Khamis, B. Kusy, C. T. Chou, and W. Hu, "Wirelax: Towards real-time respiratory biofeedback during meditation using wifi," *Ad Hoc Networks*, vol. 107, 10 2020.

[11] H. Wang, D. Zhang, Y. Wang, J. Ma, Y. Wang, and S. Li, "RT-Fall: A Real-Time and Contactless Fall Detection System with Commodity WiFi Devices," *IEEE Transactions on Mobile Computing*, vol. 16, pp. 511–526, 2 2017.

[12] S. Palipana, D. Rojas, P. Agrawal, and D. Pesch, "Falldefi," *Proceedings of the ACM on Interactive, Mobile, Wearable and Ubiquitous Technologies*, vol. 1, pp. 1–25, 1 2018.

[13] N. Bahadori, J. Ashdown, and F. Restuccia, "ReWiS: Reliable Wi-Fi Sensing Through Few-Shot Multi-Antenna Multi-Receiver CSI Learning," in *2022 IEEE 23rd International Symposium on a World of Wireless, Mobile and Multimedia Networks (WoWMoM)*. Los Alamitos, CA, USA: IEEE Computer Society, jun 2022, pp. 50–59.

[14] S. Palipana, P. Agrawal, and D. Pesch, "Channel state information based human presence detection using non-linear techniques," *Proceedings of the 3rd ACM Conference on Systems for Energy-Efficient Built Environments, BuildSys 2016*, pp. 177–186, 11 2016.

[15] J. Wang, L. Zhang, Q. Gao, M. Pan, and H. Wang, "Device-free wireless sensing in complex scenarios using spatial structural information," *IEEE Transactions on Wireless Communications*, vol. 17, pp. 2432–2442, 4 2018.

[16] L. Guo, L. Wang, J. Liu, W. Zhou, and B. Lu, "Huac: Human activity recognition using crowdsourced wifi signals and skeleton data," *Wireless Communications and Mobile Computing*, vol. 2018, 2018.

[17] W. Wang, A. X. Liu, M. Shahzad, K. Ling, and S. Lu, "Device-Free Human Activity Recognition Using Commercial WiFi Devices," *IEEE Journal on Selected Areas in Communications*, vol. 35, pp. 1118–1131, 5 2017.

[18] F. Xiao, J. Chen, X. Xie, L. Gui, L. Sun, and R. Wang, "SEARE: A System for Exercise Activity Recognition and Quality Evaluation Based on Green Sensing," *IEEE Transactions on Emerging Topics in Computing*, vol. 8, pp. 752–761, 7 2020.

[19] Q. Gao, J. Wang, X. Ma, X. Feng, and H. Wang, "CSI-Based Device-Free Wireless Localization and Activity Recognition Using Radio Image Features," *IEEE Transactions on Vehicular Technology*, vol. 66, pp. 10 346–10 356, 11 2017.

[20] J. Donahue, L. A. Hendricks, M. Rohrbach, S. Venugopalan, S. Guadarrama, K. Saenko, and T. Darrell, "Long-term recurrent convolutional networks for visual recognition and description," *IEEE Transactions on Pattern Analysis and Machine Intelligence*, vol. 39, no. 4, pp. 677–691, 2017.

[21] C. Chen, G. Zhou, and Y. Lin, "Cross-domain wifi sensing with channel state information: A survey," *ACM Comput. Surv.*, vol. 55, no. 11, feb 2023. [Online]. Available: https://doi.org/10.1145/3570325

[22] J. Snell, K. Swersky, and R. Zemel, "Prototypical Networks for Few-Shot Learning," in *Proceedings of the 31st International Conference on Neural Information Processing Systems*, ser. NIPS'17, 2017, p. 4080–4090.

[23] L. Wang, X. Bai, R. Xue, and F. Zhou, "Few-shot sar automatic target recognition based on conv-bilstm prototypical network," *Neurocomputing*, vol. 443, pp. 235–246, 2021. [Online]. Available: https://www.sciencedirect.com/science/article/pii/S0925231221004057

[24] A. Hernandez-Galvan, G. Ramirez-Alonso, and J. Ramirez-Quintana, "A prototypical network for few-shot recognition of speech imagery data," *Biomedical Signal Processing and Control*, vol. 86, p. 105154, 2023. [Online]. Available: https://www.sciencedirect.com/science/article/pii/S1746809423005876

[25] H. Larochelle, D. Erhan, and Y. Bengio, "Zero-data learning of new tasks," in *Proceedings of the 23rd National Conference on Artificial Intelligence - Volume 2*, ser. AAAI'08. AAAI Press, 2008, p. 646–651.

[26] C. H. Lampert, H. Nickisch, and S. Harmeling, "Attribute-based classification for zero-shot visual object categorization," *IEEE Transactions on Pattern Analysis and Machine Intelligence*, vol. 36, no. 3, pp. 453–465, 2014.

[27] F. Meneghello, N. Dal Fabbro, D. Garlisi, I. Tinnirello, and M. Rossi, "A CSI Dataset for Wireless Human Sensing on 80 MHz Wi-Fi Channels," *IEEE Communications Magazine*, 2023.

[28] S. Sen, B. Radunovic, R. R. Choudhury, and T. Minka, "You Are Facing the Mona Lisa: Spot Localization Using PHY Layer Information," in *Proceedings of the 10th International Conference on Mobile Systems, Applications, and Services*, ser. MobiSys '12, 2012, p. 183–196. [Online]. Available: https://doi.org/10.1145/2307636.2307654

[29] Z. Chen, L. Zhang, C. Jiang, Z. Cao, and W. Cui, "Wifi csi based passive human activity recognition using attention based blstm," *IEEE Transactions on Mobile Computing*, vol. 18, no. 11, pp. 2714–2724, 2019.

[30] G. Diaz, I. Sobron, I. Eizmendi, I. Landa, J. Coyote, and M. Velez, "Channel phase processing in wireless networks for Human Activity Recognition," *Internet of Things*, vol. 24, p. 100960, 2023. [Online]. Available: https://www.sciencedirect.com/science/article/pii/S2542660523002834

[31] D. Wang, J. Yang, W. Cui, L. Xie, and S. Sun, "Caution: A robust wifi-based human authentication system via few-shot open-set recognition," *IEEE Internet of Things Journal*, vol. 9, no. 18, pp. 17 323–17 333, 2022.

[32] X. Zhang, C. Tang, K. Yin, and Q. Ni, "Wifi-based cross-domain gesture recognition via modified prototypical networks," *IEEE Internet of Things Journal*, vol. 9, no. 11, pp. 8584–8596, 2022.

[33] F. Wang, W. Gong, and J. Liu, "On spatial diversity in wifi-based human activity recognition: A deep learning-based approach," *IEEE Internet of Things Journal*, vol. 6, no. 2, pp. 2035–2047, 2019.

[34] S. Shang, Q. Luo, J. Zhao, R. Xue, W. Sun, and N. Bao, "Lstm-cnn network for human activity recognition using wifi csi data," *Journal of Physics: Conference Series*, vol. 1883, no. 1, p. 012139, apr 2021. [Online]. Available: https://dx.doi.org/10.1088/1742-6596/1883/1/012139

[35] F. Ordóñez and D. Roggen, "Deep convolutional and lstm recurrent neural networks for multimodal wearable activity recognition," *Sensors*, vol. 16, no. 1, p. 115, Jan 2016. [Online]. Available: http://dx.doi.org/10.3390/s16010115

[36] M. T. Islam and S. Nirjon, "Wi-fringe: Leveraging text semantics in wifi csi-based device-free named gesture recognition," in *2020 16th International Conference on Distributed Computing in Sensor Systems (DCOSS)*, 2020, pp. 35–42.

[37] Y. Zhang, Y. Zheng, K. Qian, G. Zhang, Y. Liu, C. Wu, and Z. Yang, "Widar3.0: Zero-effort cross-domain gesture recognition with wi-fi," *IEEE Transactions on Pattern Analysis and Machine Intelligence*, vol. 44, no. 11, pp. 8671–8688, 2022.

[38] H. Lee, C. R. Ahn, and N. Choi, "Toward single occupant activity recognition for long-term periods via channel state information," *IEEE Internet of Things Journal*, pp. 1–1, 2023.

[39] S. Hochreiter and J. Schmidhuber, "Long Short-Term Memory," *Neural Computation*, vol. 9, no. 8, pp. 1735–1780, 1997.

[40] F. Meneghello, N. Dal Fabbro, D. Garlisi, I. Tinnirello, and M. Rossi, "A CSI Dataset for Wireless Human Sensing on 80 MHz Wi-Fi Channels," *IEEE Communications Magazine*, pp. 1–6, 2023.

[41] M. Schulz, D. Wegemer, and M. Hollick, "Nexmon: The C-based Firmware Patching Framework," https://nexmon.org, accessed: 2022-08-22.

[42] L. Van der Maaten and G. Hinton, "Visualizing data using t-SNE." *Journal of machine learning research*, vol. 9, no. 11, 2008.